JOURNAL OF MATERIALS SCIENCE 32 (1997) 129–133

Characterization of artificially patinated layers on artistic bronze exposed to laboratory SO_2 contamination

J. M. BASTIDAS, A. LÓPEZ-DELGADO, F. A. LÓPEZ
Centro Nacional de Investigaciones Metalúrgicas, CSIC, Avda. Gregorio del Amo 8, 28040 Madrid, Spain

M. P. ALONSO
Facultad de Bellas Artes, Universidad Complutense, El Greco 2, 28040 Madrid, Spain

Artificially patinated artistic bronze was exposed to the action of 0.10 and 12.68 ppm SO_2 contamination in the laboratory at 100% relative humidity. The surface layers were characterized using electrochemical, atomic absorption, X-ray powder diffraction techniques and Fourier transform–infrared spectrometry. Thermal and calorimetric studies were also performed. Some of the compounds identified were cuprite (Cu_2O), digenite ($Cu_{1.8}S$), yarrowite (Cu_9S_8), chalcocite (Cu_2S), brochantite ($Cu_4(OH)_6SO_4$), bonattite ($CuSO_4 \cdot 3H_2O$) and Sn_2S_3.

1. Introduction

Before bronze works of art are placed in a museum or outdoor environment, their surface must be suitably prepared; an example is the sulphide treatment of bronze statues [1]. The oxidation processes of bronze in aqueous solutions produce the formation of surface layers whose physical characteristics and chemical compositions depend on the nature, surface finish, heat treatment and temperature of the medium [2].

It is well known that the presence of small amounts of SO_2 emissions can cause metal deterioration, SO_2 being an accelerating corrosion factor of bronze monuments in urban and industrial areas [3, 4]. Nassau *et al.* [5, 6] pointed out that the cuprous oxide formed on copper is decomposed by the action of a significant amount of a sulphate and/or possibly a sulphide.

In recent laboratory research, the corrosion of patinated bronze in the presence of sulphur dioxide contamination in the surrounding moist air was studied, and it was concluded that little protective action was induced by patinating the bronze [7].

A study of the effect of SO_2 on copper and its alloys is of practical interest because of the large number of situations where copper materials are used. For instance, works of art, like chalcographic copper plates exposed to indoor atmospheres (museums and conservation centres) or bronze statues and copper used in architectural applications exposed to outdoor conditions, are tarnished by a patina whose protective properties are unknown [7, 8]. Because copper is a common conductor material, it is also used on circuit boards and other electronic devices where patination is an undesired process than can cause failure in equipment [9]. Finally, copper is also used in biomedical applications, like intrauterine devices (IUD), and corrosion may diminish the effectiveness of a copper IUD [10]. It is concluded that research is needed to understand the patination process on copper and its alloys in the presence of SO_2 contamination.

The aim of this work was to study the effects of simulated SO_2 contamination on artificial surface layers formed on artistic bronze in K_2S aqueous solution. In particular, to characterize the corroded bronze patinated by the effect of SO_2 at 100% relative humidity.

2. Experimental procedure

The chemical composition of artistic cast bronze was (wt %) 8 Sn, 5 Pb, balance copper. The bronze ingots were cut into 2.5 cm × 2.0 cm × 0.3 cm samples.

Mechanically polished samples were prepared with different grades of emery papers (down to 2/0). Samples were further chemically etched in a 10% HNO_3 aqueous solution for 10 min, rinsed in distilled water and heated in an oven (Selecta Model 210), held at 160 °C, for 1 h. Finally, samples were immersed in a 10 wt % K_2S solution, held at 70 °C, for 3 min. This procedure is referred to here as the artificial patination of bronze in a K_2S aqueous solution.

SO_2-contaminated atmospheres were generated in a tightly closed desiccator-type container of about 2.4 l volume. The relative humidity was approximately 100%. Two SO_2 contamination levels, 0.10 and 12.68 ppm, were studied. The high and low levels of SO_2 contamination are interesting because they supply complementary information referring to extreme cases. The temperature was maintained at 30 °C for all measurements by immersing the containers in

a thermostatically controlled water bath. Experimental details have been described elsewhere [7].

The bronze samples were exposed to the action of SO_2 for a period of 21 days. At the end of these experiments, the nature of the surface products was determined.

Hereafter, patinated bronze will be referred to as Sample O, and patinated bronze exposed to the action of 0.10 and 12.68 ppm SO_2 contamination as Samples A and B, respectively.

Electrochemical studies were performed by cathodic reduction and cathodic stripping using a Schlumberger 1286 Electrochemical Interface connected to an HP 7440A Plotter. The classic three-electrode configuration was used, employing a saturated calomel electrode (SCE) as reference and a spiral AISI 316-L stainless steel wire as the counter electrode. Experiments were carried out under static conditions at 30 °C. A 0.1 M sodium acetate solution, 350 ml, pH close to 8 and analytical grade, was used. This solution was chosen because the corrosion process is assumed to be slow enough to allow stationary conditions to be attained [11]. The solution was de-aerated by bubbling nitrogen through the system for 1 h before the start of experimentation and throughout its duration. A surface area of 1 cm^2 was the working electrode and the remainder of the sample was masked using 3M Scotchrap corrosion protection tape.

Solid phases formed on the bronze surface were characterized by X-ray powder diffraction (XRD), employing a Siemens D500 diffractometer with monochromatized CuK_α radiation.

Chemical analysis was performed by atomic absorption spectroscopy employing a Philips spectrophotometer (Pye Unicam SP9).

Infrared spectra were recorded in the 4000–400 cm^{-1} region using a Nicolet Magna 550 Fourier transform–infrared (FTIR) spectrophotometer, in transmission mode. Samples were prepared by mixing with cesium iodine.

Calorimetric studies were performed up to 750 °C using a Shimadzu DSC 50 differential scanning calorimeter. Thermogravimetric (TG) curves were obtained up to 1100 °C by means of a Shimadzu TGA-50H unit. All tests were carried out in flowing air (20 ml min^{-1}) and at a heating rate of 20 °C min^{-1}, with a 15 mg quantity of the samples.

3. Results and discussion

Cathodic reduction curves for Samples O, A and B are depicted in Fig. 1. On Sample O (Fig. 1a) only one main broad ill-defined peak is observed close to − 1.2 V/SCE which could be attributed to the reduction of cuprous sulphide [12, 13]. Similar results with copper showing poorly resolved peaks have been attributed to a thick coating of oxide on copper [14]. Thus, the considerable thickness of copper sulphide layers could contribute to the poor resolution of this peak. For Sample A (Fig. 1b), a first cathodic peak can be observed at about − 0.7 V/SCE for cuprous oxide. A small doublet is formed more cathodically at about − 1.1 V/SCE for cuprous sulphide, which probably could be attributed to a different stequiometric cuprous sulphide. Finally, for Sample B (Fig. 1c) two main ill-defined peaks can be observed at − 0.6 and − 1.1 V/SCE, corresponding to cuprous oxide and sulphide, respectively.

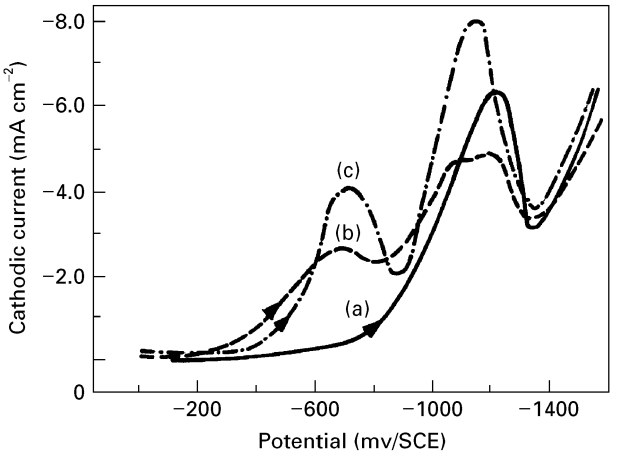

Figure 1 Reduction scans in 0.10 M de-aerated sodium acetate solution for Samples (a) O, (b) A and (c) B obtained at a potential sweep rate of 5 mV s^{-1} starting at the open circuit potential.

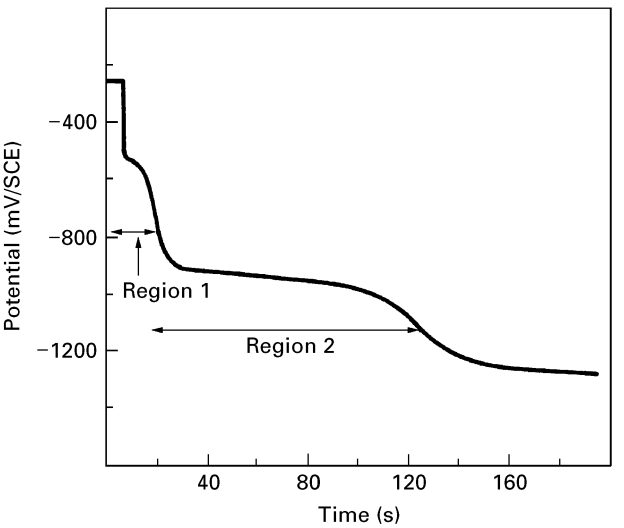

Figure 2 Cathodic stripping for artificially patinated bronze (Sample O) in 0.10 M de-aerated sodium acetate solution. $i = 2.8$ mA cm^{-2}.

Fig. 2 shows the recorded potential versus time curve for the cathodic stripping of Sample O in a 0.1 M de-aerated sodium acetate solution. Two reduction regions are presented. Region 1 was defined by a drop in potential followed by a small plateau, in turn followed by an inflection point. An extensive plateau, Region 2, was formed before the second inflection point, after which hydrogen bubbles appeared on the bronze surface and the potential stabilized, an indication that all the products on bronze have been reduced and that the bronze surface was being cleaned. The layer thickness was determined using Faraday's law [15]. The thickness data were calculated assuming the average density of oxide layers in Region 1 to be equal to that of cuprous oxide, and in Region 2 to cuprous sulphide. Despite a lack of information about the surface roughness factor of the samples, the thickness under conditions apertaining to

Fig. 2 was approximately 52 nm for cuprous oxide and 407 nm for cuprous sulphide. The information from Fig. 2 is useful from a practical point of view for calculating the surface pH values from the Pourbaix diagrams.

The results in Fig. 2, as well as the information supplied in Fig. 1a, indicate the presence of cuprous oxide. This apparent contradiction could be attributed to the inertia caused by the thickness of the patina–bronze system. X-ray diffraction (XRD) analyses were carried out to explain these results.

Fig. 3 shows the XRD patterns of Samples O, A and B. The crystalline phases observed on Sample O (Fig. 3a) are cuprite (Cu_2O) and two copper sulphides: digenite ($Cu_{1.8}S$) and yarrowite (Cu_9S_8). The $d_{hkl} = 0.2839$ nm diffraction maximum corresponding to the most intense peak of Sn_2S_3 was also observed. Given the poor crystallinity of Sample O, the high intensity of this peak could be attributed to preferential crystal orientations. The XRD pattern of Sample A (Fig. 3b) shows that the principal crystalline phase developed is chalcocite-Q ($Cu_{1.96}S$) along with yarrowite and cuprite. The diffractogram for Sample B (Fig. 3C) consists of crystalline phases: chalcocite (Cu_2S), brochantite ($Cu_4(OH)_6SO_4$), bonattite ($CuSO_4 \cdot 3H_2O$), Sn_2S_3 and cuprite. Peaks corresponding to yarrowite are not observed.

The presence of brochantite and bonattite was confirmed by FTIR analysis. Table I summarizes the assignment of FTIR bands of Sample B according to the literature [16, 17].

The identification of tin sulphide by XRD analysis was confirmed by atomic absorption chemical analysis carried out on Sample O in the 0.1 M sodium acetate solution after cathodic reduction experiments; the results were 67.5% Cu, 5.7% Sn and 0.8% Pb. The low lead content explained the absence of lead peaks in Fig. 1. It is difficult to explain the absence of tin reduction peaks around -700 mV/SCE [18]. However, it is possible that the high copper content conceals tin reduction peaks.

A calorimetric study was carried out to confirm the above XRD results. DSC curves recorded for Samples O, A and B are shown in Fig. 4. For Sample O (Fig. 4a) a first exothermic peak is observed at 366 °C (T_{max}) with a shoulder at 345 °C. The CuS oxidation

$$CuS(s) + 2O_2(g) \rightarrow CuSO_4(s)$$

$$\Delta H = -171.1 \text{ kcal mol}^{-1} \qquad (1)$$

takes place between 340 and 400 °C [19]. Because of that, the observed effect could correspond to the oxidation of yarrowite. The XRD pattern for Sample O heated at 380 °C, although quite amorphous, consists of digenite and $CuSO_4$. The presence of $CuSO_4$ was confirmed by FTIR, bands of the vibrational modes appeared at 1099, 966 and 497 cm^{-1} corresponding to ν_3, ν_1 and ν_4, respectively [16]. After that, two other exothermic effects, centred at 447 and 497 °C, were observed. These poor intensity peaks are partially overlapped and could be attributed to the oxidation of both cuprous sulphide (digenite) [20, 21] and tin sulphide.

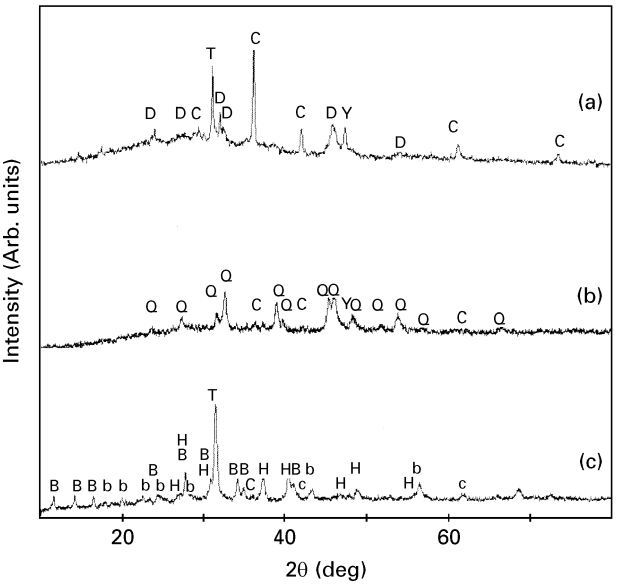

Figure 3 XRD patterns of Samples (a) O, (b) A and (c) B (D-digenite; C = cuprite; T = Sn_2S_3; Y = yarrowite; Q = chalcocite-Q; B = brochantite; b = bonattite; H = chalcocite).

TABLE I Infrared absorption band frequencies of Sample B

(cm^{-1})[a]	Assignation
3588 sh, 3543 sh	ν_{OH}
3445 b, s	ν_{H_2O}
1620 w	δ_{HOH}
1232 m, 1096 vs	ν_3 SO_4
1037 m, 990 m	ν_1 SO_4
919 w	δ_{OH}
783 w	ρ_{H_2O}
614 s	ν_4 SO_4
484 m	ν Cu–O

[a] sh = shoulder, b = broad, s = strong, m = medium, vs = very strong, w = weak.

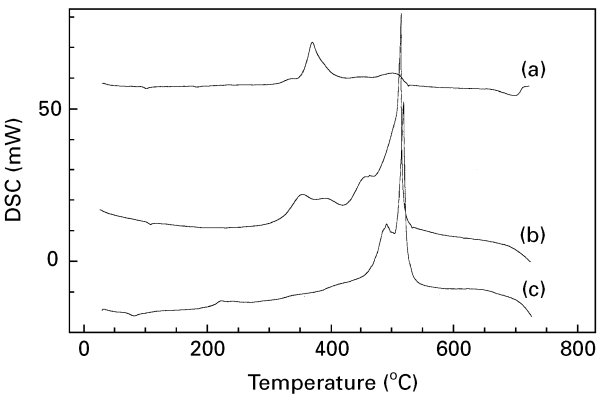

Figure 4 DSC curves of Samples (a) O, (b) A and (c) B.

The crystalline phases identified in the XRD pattern recorded on Sample O heated at 550 °C were $CuSO_4$, $CuO \cdot CuSO_4$ and CuO. Weak peaks corresponding to cuprite were also observed. The presence of

$CuO \cdot CuSO_4$ and CuO can be explained by the reactions

$$Cu_2S(s) + 5/2O_2(g) \rightarrow CuO \cdot CuSO_4(s)$$
$$\Delta H = -199.7 \text{ kcal mol}^{-1} \quad (2)$$
$$Cu_2S(s) + 5/2O_2(g) \rightarrow CuO(s) + CuSO_4(s)$$
$$\Delta H = -201.5 \text{ kcal mol}^{-1} \quad (3)$$

which may occur consecutively or simultaneously. Finally, Fig. 4a shows an endothermic peak about 700 °C due to the decomposition process of $CuSO_4$

$$2CuSO_4(s) \rightarrow CuO \cdot CuSO_4(s) + SO_3(g)$$
$$\Delta H = 53.73 \text{ kcal mol}^{-1} \quad (4)$$

The XRD diffractogram of Sample O heated at 700 °C consists of crystalline phases $CuO \cdot CuSO_4$, CuO, Cu_2O and SnO_2; this latter compound formed in the previous step but was not observed until here. An intensive peak appears at $d_{hkl} = 0.2618$ nm which can be attributed to (i) K_2S proceeding from the artificial patination process, or (ii) $CuO \cdot 3H_2O$ proceeding from the subsequent hydration of the sample.

The decomposition process of Sample A occurs in a similar way to that described for Sample O. In the DSC curve, Fig. 4b, the exothermic peaks observed between 330 and 400 °C correspond to yarrowite oxidation, as in Reaction 1, and the peaks which appeared between 425 and 500 °C correspond to the oxidation of both cuprous sulphide (chalcocite-Q, in this case) in Reactions 2, 3 and tin sulphide.

The DSC curve for Sample B (Fig. 4c) shows a weak first endothermic peak between 62 and 91 °C; this is attributed to the dehydration process of bonattite

$$CuSO_4 \cdot 3H_2O \rightarrow CuSO_4 + 3H_2O \quad (5)$$

This process involves a weight loss as shown in the TG curve depicted in Fig. 5. A second step takes place between 175 and 230 °C also with a weight loss, accompanied by the exothermic effect in this temperature range on the DSC curve ($T_{max} = 222$ °C). The dehydroxylation process of brochantite

$$Cu_4(OH)_6SO_4 \rightarrow CuSO_4 + 3CuO + 3H_2O \quad (6)$$

may occur in this step.

The XRD pattern of Sample B heated at 230 °C consists of $CuSO_4$, CuO and Cu_2S in accordance with Reaction 6. Peaks are not observed in the temperature range corresponding to cupric sulphide oxidation processes on either the DSC or the TG curves.

The oxidation of cuprous sulphide (chalcocite, in this case) and tin sulphide in Sample B, takes place in a similar way and in the same temperature range as Samples O and A.

The decomposition of $CuSO_4$, Reaction 4, occurs in Samples A and B at a higher temperature than on Sample O. Only the beginning of this process can be seen in DSC curves (Fig. 4a, b) owing to equipment limitations. However, the TG curve of Sample B shows a great weight loss taking place between 680 and 850 °C, and its asymmetrical derivative peak

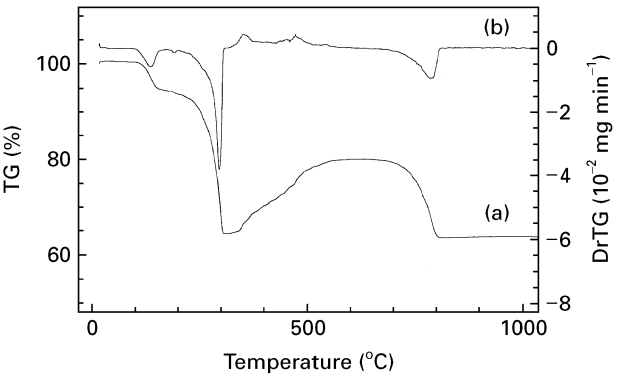

Figure 5 (a) TG and (b) DrTG curves of Sample B.

(DrTG) could be due to the decomposition of both $CuSO_4$, Reaction 4, and $CuO \cdot CuSO_4$

$$CuO \cdot CuSO_4(s) \rightarrow 2CuO(s) + SO_3(g)$$
$$\Delta H = 50.12 \text{ kcal mol}^{-1} \quad (7)$$

overlapping. XRD patterns recorded on Samples A and B, heat treated at 850 °C consist of tenorite, cuprite and cassiterite.

4. Conclusion

The artificial patination process with K_2S aqueous solution on artistic bronze surfaces produces layers of different types of copper sulphides on the cuprite layer. Bearing in mind the complex CuS–Cu_2S system, these sulphides could be named, in a generic manner, cupric sulphides if the developed phase is similar to CuS, e.g. yarrowite, and cuprous sulphides, if it is similar to Cu_2S, e.g. digenite, chalcocite-Q and chalcocite.

The exposure of artificial as-patinated bronze surfaces to the action of laboratory SO_2 contamination originates compounds depending on the SO_2 concentration. According to the results, a low sulphur dioxide contamination level (0.10 ppm) causes modifications of crystalline phases in these working conditions. At the high level of contamination (12.68 ppm), copper hydroxisulphates and sulphates form, possibly at the expense of the initial layer of cupric sulphides. Although the influence of the artificial patina on tin is shown by XRD, it has not been possible to observe its effects on lead.

Acknowledgement

The authors thank the Comunidad Autónoma de Madrid (C226/90) for financial support.

References

1. T. E. GRAEDEL, K. NASSAU and J. P. FRANEY, *Corros. Sci.*, **27** (1987) 639.
2. G. BRUNORO, G. GILLI and R. NAGLIATI, *Surf. Technol.* **21** (1984) 125.
3. E. MATTSSON and R. HOLM, "Metal Corrosion in the Atmosphere", ASTM STP 435 (American Society for Testing and Materials, Philadelphia, PA, 1968) p. 187.

4. N. HJELM-HANSEN, *Stud. Conserv.* **29** (1984) 17.
5. K. NASSAU, P. K. GALLAGHER, A. E. MILLER and T. E. GRAEDEL, *Corros. Sci.* **27** (1987) 669.
6. K. NASSAU, A. E. MILLER and T. E. GRAEDEL, *ibid.* **27** (1987) 703.
7. J. M. BASTIDAS, M. P. ALONSO, E. M. MORA and B. CHICO, *Werkst. Korros.* **45** (1995) 515.
8. E. OTERO, J. M. BASTIDAS, W. LOPEZ and J. L. G. FIERRO, *ibid.* **45** (1994) 387.
9. R. B. COMIZZOLI, J. P. FRANEY, T. E. GRAEDEL, G. W. KAMMLOTT, A. E. MILLER, A. J. MULLER, G. A. PEINS, L. A. PSOTA-KELTY, J. D. SINCLAIR and R. C. WETZEL, *J. Electrochem. Soc.* **139** (1992) 2058.
10. J. M. BASTIDAS and J. SIMANCAS, Characterization of Corrosion Products on a copper-containing intrauterine device during storage at room temperature. Submitted to *Biomaterials* 1996.
11. M. LENGLET, K. KARTOUNI and D. DELAHAYE, *J. Appl. Electrochem.* **21** (1991) 697.
12. C. FIAUD and N. GHIMOUZ, *Br. Corros. J.* **24** (1989) 279.
13. J. VEDEL and M. SOUBEYRAND, *J. Electrochem. Soc.* **127** (1980) 1730.
14. R. L. DEUTSCHER and R. WOODS, *J. Appl. Electrochem.* **16** (1986) 413.
15. U. R. EVANS, "Metallic Corrosion Passivity and Protection" (E. Arnold, London, 1948) p. 64.
16. H. LANGFEKDEROVÁ, M. LINKESOVÁ, M. SERATOR and J. GAZO, *J. Thermal Anal.* **17** (1979) 107.
17. H. KADAMA, "Infrared Spectra of Minerals", 1st edn (Minister of Supply and Services, Ottawa, Ontario, Canada, 1985).
18. E. DELTOMBE, N. DE ZOUBOV, C. VANLEUGENHAGHE and M. POURBAIX, "Atlas of Electrochemical Equilibria in Aqueous Solutions" (Pergamon, London, 1966) p. 475.
19. S. E. KHALAFALLA and I. D. SHAH, *Metall. Trans.* **1** (1970) 2151.
20. M. E. WADSWORTH, K. L. LEITER, W. H. PORTER and J. R. LEWIS, *ibid.* **218** (1960) 519.
21. J. R. LEWIS, J. H. HAMILTON, J. C. NIXON and C. L. GRAVERSEN, *Trans. TMS-AIME* (1948) 2388.

Received 31 May 1995
and accepted 2 July 1996